44th AIAA/ASME/SAE/ASEE Joint Propulsion Conference & Exhibit
21 - 23 July 2008, Hartford, CT

AIAA 2008-4689

Simulation Of Blast Wave Propagation and Particle Motion from Detonation Containing Dense Inert Particles

Kaushik Balakrishnan* and Suresh Menon†

Computational Combustion Laboratory

School of Aerospace Engineering

Georgia Institute of Technology

Atlanta, GA 30332

I. Abstract

The propagation of an explosive blast wave containing dense inert metal particles is studied numerically by means of a three-dimensional simulation. A robust two-phase methodology is used with appropriate models to account for real gas behavior, inter-phase interactions, and inter-particle collisions to study the problem of interest. The velocity and momentum profiles of the gas and particle phases are studied elaborately and used to elucidate the underlying physics. The impulse characteristics of heterogeneous explosives are compared with a homogeneous explosive containing the same amount of the high explosive. It is observed that the addition of solid particles augments the impulsive loading significantly in the near-field, and to a smaller extent in the far-field. Insight into the effect of particle loading on the shock propagation characteristics as well as particle motion is also obtained from these studies.

II. Introduction

The problem of detonation of explosives containing solid (inert or reactive) particles, although limited, has been studied both experimentally and numerically in the past. Lanovets et al.[1] performed a numerical study based on a two-fluid approach and reported that for a certain range of particle size and density, the solid particles can catch up with the shock front and overtake it. Milne[2] developed a simple model to study detonation of a nitromethane charge with inert particles using a simple one step Arrhenius kinetics. Zhang et al.[3] carried out experimental and numerical studies to obtain the shock front and particle cloud trajectories for a nitromethane charge containing steel particles. They concluded that for spherical and cylindrical charges, the possibility of the solid particles overtaking the shock front exists, but is highly unlikely for planar charges due to their lower attenuation rates. They also reported that the distance required for the particles to overtake the shock front strongly depends on the charge size and material density, but weakly on the solid volume fraction. They also concluded that a particle size limit exists, above which the distance required for the particles to penetrate the shock front is less sensitive to the particle size and below which, the distance required depends on particle size. Zhang et al.[4] reported that the momentum transfer from an explosive to the solid particles during the particle crossing of the detonation front is insignificant for heavy-metal and significant for light-metal particles.

Some numerical effort has also been undertaken to evaluate impulsive loading from a heterogeneous charge comprising of a high explosive and inert/reacting solid particles. Frost et al.[5] carried out a combined experimental and numerical study focusing on particle momentum and impulse effects of a nitromethane charge with steel particles. They showed that the integrated particle momentum flux is larger than the gas momentum flux by a factor of about 3–4 in the near field. They concluded that the impulsive load on a near-field structure was increased by a factor of 2 for a heterogeneous charge. Massoni et al.[6] proposed a

*PhD Candidate, AIAA Student Member
†Professor, AIAA Associate Fellow

Copyright © 2008 by Kaushik Balakrishnan and Suresh Menon. Published by the American Institute of Aeronautics and Astronautics, Inc., with permission.

reactive model for aluminized explosive charges in spherical coordinates. They used an ALE method to track the interface between the detonation products and the surrounding with a detonation tracking technique for the initialization.

In the present study, the multi-phase equations are solved by the Discrete Equations Method (DEM), originally proposed by Abgrall & Saurel[7] for dense particle phase modeling within a two-fluid approach. The scheme is robust in nature and can handle shock interactions with volume fraction discontinuities. Chinnayya et al.[8] extended the DEM to study detonation waves in heterogeneous energetic materials. Their methodology used the pure material equations of state, instead of a mixture equation of state, highlighting the robust nature of the DEM. Le Metayer et al.[9] extended the DEM to handle evaporation fronts. In the original DEM used by these authors, the gas and solid phases were treated Eulerian in nature. In the current approach, the solid particles are tracked using Lagrangian tracking, and this requires an extension of the DEM to an Eulerian-Lagrangian formulation. The differences between the original Eulerian-Eulerian DEM and the Eulerian-Lagrangian DEM are also highlighted in this paper.

This study is aimed at providing insight into the fundamental physics of detonation processes, dense particle modeling and dispersion, with a focus on inert particles. This paper is organized as follows. In Section III, the governing equations and the numerical methodology are discussed. In Section IV, the results and discussions are presented for the multi-phase blast wave problem, as well as for canonical studies used to verify the solver. Finally, in Section V, the conclusions drawn from this study are presented.

III. Governing Equations and Numerical Method

III.A. Gas-phase

The gas phase Navier-Stokes equations, applicable in dense two-phase flow scenarios in the abscence of body forces are

$$\frac{\partial}{\partial t}\begin{bmatrix} \alpha_g\rho_g \\ \alpha_g\rho_g u_{g,i} \\ \alpha_g\rho_g E_g \\ \alpha_g\rho_g Y_{g,k} \end{bmatrix} + \frac{\partial}{\partial x_j}\begin{bmatrix} \alpha_g\rho_g u_{g,j} \\ \alpha_g\rho_g u_{g,i}u_{g,j} + \alpha_g p_g\delta_{ij} - \alpha_g\tau_{g,ij} \\ \alpha_g\left(\rho_g E_g + p_g\right)u_{g,j} - \alpha_g u_{g,i}\tau_{g,ji} + \alpha_g q_{g,j} \\ \alpha_g\rho_g Y_{g,k}\left(u_{g,j} + V_{g,j}\right) \end{bmatrix} = \begin{bmatrix} 0 \\ p^*\frac{\partial\alpha_g}{\partial x_j}\delta_{ij} - \tau_{ij}{}^*\frac{\partial\alpha_g}{\partial x_j} \\ p^* u_j{}^*\frac{\partial\alpha_g}{\partial x_j} - u_i{}^*\tau_{ij}{}^*\frac{\partial\alpha_g}{\partial x_j} \\ \dot{\omega}_k \end{bmatrix} + \begin{bmatrix} \dot{\rho}_p \\ \dot{F}_{p,i} \\ \dot{Q}_p + \dot{W}_p \\ \dot{S}_{p,k} \end{bmatrix} \tag{1}$$

where α_g denotes the gas phase volume fraction, ρ_g the density, $u_{g,i}$ the i-th component of velocity, E_g the total energy given by the sum of the internal (e_g) and kinetic energies, $e_g + \frac{1}{2}u_{g,i}u_{g,i}$, and $Y_{g,k}$ the mass fraction of the k-th species. The stress tensor is denoted by $\tau_{g,ij}$, the j-direction heat flux by $q_{g,j}$, the j-component diffusion velocity by $V_{g,j}$, and the chemical production of the k-th species by $\dot{\omega}_k$. Since the problem of interest involves high speed flow, the diffusion time scales are generally at least an order of magnitude higher than the convective time scales. Thus, the diffusion terms, viz. $\tau_{g,ij}$ and $V_{g,j}$ are neglected in this study.

Also, p^* and $u_i{}^*$ denote respectively, the pressure and i-th component of velocity at the interface between the two phases. The interface stress tensor is denoted by $\tau_{ij}{}^*$, and is neglected using the same assumption that diffusion time scales are large for the present problem of study. The last term on the right side identifies the inter-phase coupling terms: mass transfer $\dot{\rho}_p$, i-th component momentum transfer $\dot{F}_{p,i}$, heat transfer $\dot{Q}_p$, work transfer $\dot{W}_p$, and chemical production of k-th species $\dot{S}_{p,k}$. These terms are evaluated using Lagrangian tracking of solid particles, and are discussed later. To account for real gas behavior, the JWL Equation of state is solved for the detonation products using the constant specific heat at constant volume (C_v) approach[10] to obtain a thermal form of the equation of state.

$$p_g = A\,exp\left(\frac{-R_1\rho_o}{\rho_g}\right) + B\,exp\left(\frac{-R_2\rho_o}{\rho_g}\right) + \omega\rho_g C_v T_g, \tag{2}$$

where T_g denotes the gas temperature; A, B, R_1, R_2 and ω denote JWL constants, and ρ_o, the explosive density.[11]

The gas-phase governing equations are solved using the HLLC approximate Riemann solver[12] with MUSCL reconstruction. This ensures second order accuracy in space and time. In the near-field, the dense nature of the flow-field necessisates the use of a multi-phase model. To this end, the Discrete Equations Method (DEM)[7–9] is used. The DEM is a robust multi-phase method well suited for multi-phase flows involving shocks and solid particles. The basic idea behind the method starts with the representation of the volume fraction field. Similar to the representation of flow variables to be piecewise constant in any Godunov scheme, the volume fraction field is represented in a similar manner. This is shown in in Fig. 1 for three cells containing different number of particles, and therefore different volume fractions.

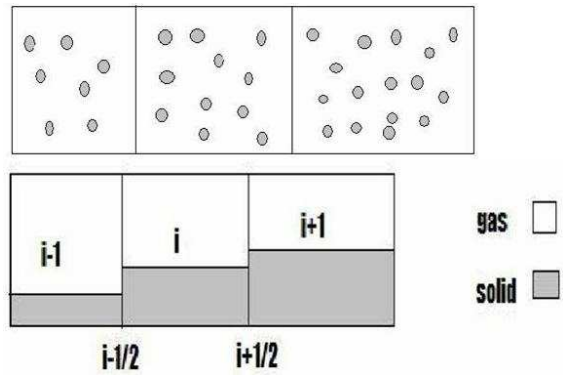

Figure 1. Volume fraction field representation in DEM.

However, the DEM formulation used in this research effort requires some alterations. In the original DEM, both phases are treated as Eulerian, and a volume fraction equation is solved to obtain the volume fraction field for each phase. In the current research effort, the solid particles are tracked using Lagrangian tracking (discussed in the next sub-section), and this requires changes to the original DEM approach. In the current approach, since the locations of each particles are known precisely, the solid volume fraction field (α_p) is obtained by volume averaging all the particles in each finite volume cell. This is used to compute the gas volume fraction field (α_g), using the equation $\alpha_g = 1 - \alpha_p$. In the original DEM, the flux for both phases are computed assuming both phases to be in continuum and the Riemann problem is solved at each gas-solid interface due to the compressible nature of each phase. The interface pressure and velocity are obtained as solutions to the Riemann problem. In the current methodology, the DEM approach is used only to compute the gas phase flux. The fluxes at gas-gas interfaces (inter-cell interfaces) are obtained in the conventional way, with the use of a Riemann solver. Since the solid particles are assumed incompressible, this requires the solution of half-Riemann problems at gas-solid interfaces. By half-Riemann problem, we refer to the Riemann problem where the compression or rarefaction wave propagates only on one side of the interface, viz. the side of the gas. The fluxes obtained from the gas-gas and gas-solid interfaces are summed up, following the same approach as in the original DEM.[7,8] Since the solid particle velocity is known at the beginning of each time step, the interface velocity at each gas-solid contact is equated to the average solid particle velocity corresponding to the cell, due to the incompressible assumption of the solid particles. The interface pressure is then obtained with the use of (a) Shock and Hugoniot relations for a compression or (b) Riemann invariants and isentropic relations for a rarefaction, as the case may be. Thus, the numerical methodology is closed and renders the system of equations to be computationally tractable. However, the Eulerian-Lagrangian DEM suffers one drawback as compared with its counterpart Eulerian-Eulerian DEM. While the latter can handle solid volume fractions from near zero to near unity, the former is strictly restricted to multi-phase flows where the solid volume fraction is less than a certain upper bound (say, 0.7). This is due to the non-continuum assumption of the solid particles, which requires a finite amount of gas to exist in each finite volume cell at all times.

III.B. Solid-phase

For the solid phase, Lagrangian tracking is used to compute the particle velocity vector ($u_{p,i}$) from the forces acting on a particle. Since the number of particles to be tracked can be very large under some scenarios, the concept of parcel is employed. Here, a parcel represents a group of particles, each corresponding to the same position and velocity vectors, and temperature. The number of parcels is chosen based on various factors such as computational cost, and available memory, and the number of particles to be assigned to a

parcel is chosen based on the desired volume fraction/mass loading. The particle position vector ($x_{p,i}$) is obtained from the velocity vector. These equations are summarized below for the circumstance involving no inter-phase mass transfer.

$$\frac{dx_{p,i}}{dt} = u_{p,i}, \tag{3}$$

$$m_p \frac{du_{p,i}}{dt} = \frac{\pi}{2} {r_p}^2 C_D \rho_g |u_{g,i} - u_{p,i}| \left(u_{g,i} - u_{p,i}\right) + m_p A_{c,i}, \tag{4}$$

where m_p is the particle mass, r_p is the particle radius, and $A_{c,i}$ is the i-component of net acceleration/deceleration on a particle due to inter-particle collisions.[13,14] The particle mass m_p is obtained as $4/3\pi {r_p}^3 \rho_p$, where ρ_p is the solid particle material density. In the above equation, C_D represents the drag coefficient and is usually expressed as empirical functions of Reynolds number, Mach number and solid volume fraction. Several different drag laws have been proposed in literature, each being unique to a specific multi-phase problem. To the best of our knowledge, no universally accepted drag law is available in literature, applicable for all kinds of multi-phase problems, i.e., dilute and dense, low and high speed. Thus, we will use different drag laws for different problems in this paper, depending on the regime of application.

Due to the dense nature of the problem, Snider's collision model[13,14] is used to compute the inter-particle collision force. This inter-particle collision force is as a result of the constant collision/contact between particles. The dynamic compaction involved in granular explosives results in these terms, and thus a collision/contact model, like the one used here, is essential to model dense two-phase explosives. More details on dynamic compaction can be found elsewhere.[15] In the collision/contact model used in this study,[13,14] the inter-particle collision force is obtained as an empirical function of the solid volume fraction. This inter-particle force is obtained from the inter-particle stress (τ) given by

$$\tau = \frac{P_s {\alpha_p}^{\beta}}{\alpha_{cs} - \alpha_p}, \tag{5}$$

where P_s (units of pressure) and β are model coefficients, and α_{cs} is the solid volume fraction at close packing. The particle acceleration/deceleration due to inter-particle collision is obtained as a gradient of the inter-particle stress using the equation

$$A_{c,i} = -\frac{1}{\alpha_p \rho_p} \frac{\partial \tau}{\partial x_i}. \tag{6}$$

The heat transfer between the two phases is estimated assuming only convection and neglecting radiation, and is used to obtain the particle temperature (T_p)

$$m_p C_p \frac{dT_p}{dt} = 2\pi r_p \kappa_g Nu \left(T_g - T_p\right), \tag{7}$$

where C_p is the specific heat of the solid particle, κ_g is the thermal conductivity of the gas phase. The Nusselt number (Nu) is typically expressed as empirical functions of Reynolds number and Prandtl number in the literature. The particle-particle collision model could, in theory, also play a role in the particle temperature equation. Particle collisions can cause velocity fluctuations, and this can give rise to the so called "granular temperature". This granular temperature is due to shear in particle collisions, during which energy dissipation can occur due to inelastic collisions.[16] This effect is neglected for the time being, with the assumption that convection is the only dominant heat transfer mechanism between the two phases.

The system of governing equations for the solid-phase are solved using a 4th order Runge-Kutta scheme to obtain the solid particle position vector, velocity vector and temperature. The coupling terms that appear on the right side of the gas phase governing equations (Eqn. 1) are obtained by volume averaging over all the particles/parcels in a finite volume (Vol) and are given by

$$\dot{F}_{p,i} = \frac{1}{Vol} \sum_{1}^{N} n_p \left[\frac{\pi}{2} {r_p}^2 C_D \rho_g |u_{p,i} - u_{g,i}| \left(u_{p,i} - u_{g,i}\right)\right], \tag{8}$$

where N is the total number of parcels in a finite volume cell and n_p is the number of particles per parcel.

$$\dot{Q}_p = \frac{1}{Vol} \sum_{1}^{N} n_p \left[2\pi r_p \kappa_g Nu \left(T_p - T_g\right)\right], \tag{9}$$

$$\dot{W}_p = \frac{1}{Vol}\sum_{1}^{N} n_p \left[\frac{\pi}{2} {r_p}^2 C_D \rho_g |u_{p,i} - u_{g,i}| \left(u_{p,i} - u_{g,i}\right) u_{p,i}\right]. \tag{10}$$

Since no inter-phase mass transfer is assumed in this study, $\dot{\rho}_p$ and $\dot{S}_{p,k}$ are neglected. The inter-particle collision can, in theory, also affect the gas phase. While collisions between gas molecules are responsible for viscosity and temperature in the gas phase, collisions between solid particles can also cause similar effects.[16] However, in the present study, the solid particles are very large, and the time scales associated with inter-particle collision is several orders of magnitude larger than those associated with inter-molecular collision in the gas phase, thus we neglect the effect of inter-particle collisions on the gas phase.

III.C. Initial detonation profile

The detonation initial profiles were obtained from Dr Doug Nance (Eglin Air Force Base).[17] This is based on a one-dimensional Direct Numerical Simulation (DNS) employing the Gas-Interpolated-Solid Stewart-Prasad-Asay (GISPA) method for the detonation process.[18] This method permits time-accurate simulation of detonation from the time of the initial shock through the completion of the explosive burn. The robustness of the GISPA algorithm is emphasized by its ability to capture the reaction zone as well as the Von Neumann spike. The GISPA method is based upon the reactive Euler equations[19]

$$\frac{\partial \vec{U}}{\partial t} + \frac{\partial \vec{F}}{\partial x} = \vec{S}_G + \vec{S}_{Rx}, \tag{11}$$

where $\vec{U} = (\rho, \rho u, E, \rho\lambda)^T$ is the vector of conserved variables. Here, λ denotes the reaction progress state variable, and $\vec{F}$ is the flux vector $\vec{F} = (\rho u, \rho u^2 + p, u(\rho E + p), \rho u \lambda)^T$. The source term $\vec{S}_G$ in (11) mathematically corrects the one-dimensional equations for non-planar coordinate systems[18]

$$\vec{S}_G = -\frac{j}{x}(\rho u, \rho u^2, u(E+P), \rho u \lambda)^T. \tag{12}$$

where x denotes distance, and j is set to 0 for planar, 1 for cylindrical, and 2 for spherical. The progress of the detonation is governed by a reaction rate expression r_x, which can take different forms for different explosives.[20] The equations (11) through (12) are solved with the use of appropriate equations of state for both the condensed explosive and the detonation products.[18] For the condensed explosive, the Hayes equation of state is used,[21] while the JWL equation of state is used for the detonation products. The Glaister's[22] version of the Roe scheme is used with MUSCL reconstruction for solving the equations to obtain the initial detonation profile.

The detonation initialization based on the GISPA method is more realistic than other ways of initialization, such as the "programmed burn" algorithm,[23] and the constant volume explosion initialization.[3] In the programmed burn algorithm, the detonation wave speed needs to be known *apriori*, which may not always be the case. In the constant volume explosion initialization, since the pressure field is assumed constant, the early momentum transfer characteristics from the gas to the particles can be erroneous. Since the GISPA algorithm is based on first principles, we believe that this initialization is more realistic than the other procedures.

IV. Results and Discussion

The simulation code is a well established solver suited for DNS/LES of combustion/turbulent liquid-gas flows.[24] The solid phase solver and the JWL equation of state are new additions to the hydrocode, and thus many canonical studies have been completed to establish the accuracy of the new algorithms. Some key results of these studies are presented first before addressing the problem of interest.

IV.A. Particle dispersion in a shock tube

Particle dispersion due to passage of a shock wave is a canonical test case to establish the ability of the solver to capture particle motion and dispersion (which requires proper drag modeling) during shock-particle interaction. The dispersion of a nylon particle ($\rho_p = 1170$ Kg/m^3) 2 mm dia. subjected to a Mach 1.56 shock is investigated repeating an earlier experimental and numerical study by Devals et al.,[25] who concluded that the particle trajectory and the velocity agree with the drag law of Igra & Takayama.[26] Initialization is based

on a high pressure region, released at zero time and allowed to expand. A domain of 3.75 m in the axial direction and a cross-section of 8 cm x 8 cm is discretized using a grid of size 375x8x8. No flux boundary conditions are used on the shock tube walls. The particle trajectory and the velocity evolution with time are shown in Fig. 2(a) and (b). The present study agrees well with the measured data and is consistent with other model predictions of similar test cases. Since this shock tube does not have an outlet, the shock reflects from the end wall, which causes the particle velocity to level off at later times (> 3 msec), and the particle trajectory to follow a near-straight line.

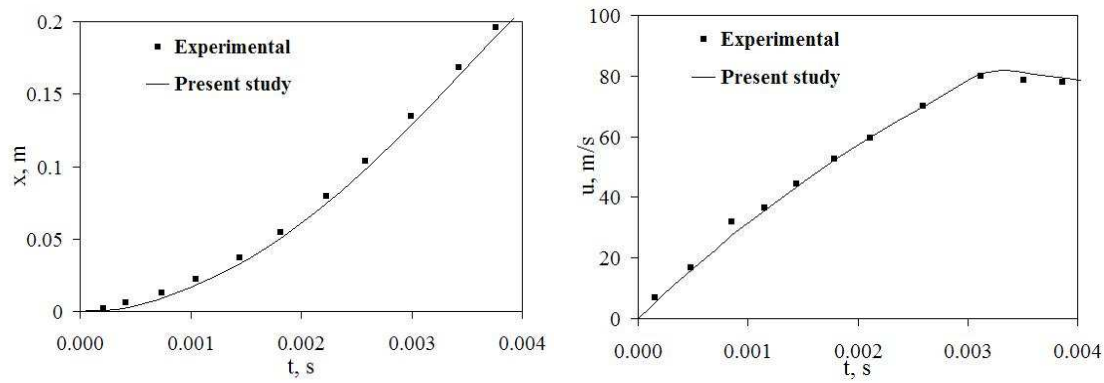

(a) (b)

Figure 2. Evolution of particle (a) trajectory and (b) velocity with time.

IV.B. Shock propagation through dust-gas suspension

The attenuation of a shock wave upon its passage through a dilute gas-particle mixture is also studied using a drag law applicable for this regime.[27] This is a well established test case studied earlier using both experiments and numerical modeling.[28] A shock wave of a prescribed Mach number, $M_s = 1.49$ passes through a cloud of glass particles (27 μm dia, $\rho_p = 2500$ Kg/m^3) initially occupying a mass loading ratio, $\eta = 0.63$. The same shock tube geometry[28] is simulated using a no-flux boundary condition in the shock tube walls, and supersonic outflow in the low pressure region. Initialization is achieved by means of a high pressure region that is then allowed to expand. Although the experiments were performed in a circular cross-section shock tube,[28] we used a square cross-section, which should not affect the results due to the one-dimensionality of the problem. A shock tube 7.81 m long is considered, with a cross section being a square of side 5 cm, and is resolved using a 781x10x10 grid. Fig. 3 shows the shock wave Mach number as it propagates through the gas-particle mixture. Also shown are the attenuation rates obtained by Aizik et al.,[29] and numerical results obtained by other investigators.[30] The shock wave attenuation predicted by the present hydrocode is in good agreement with other studies.

IV.C. Shock propagation through dense gas-particle mixture

In order to validate the Eulerian-Lagrangian DEM approach implemented in the code, the problem of shock wave propagation through a dense gas-particle mixture is investigated and compared to available experimental data.[31] The propagation of a Mach 1.3 shock into a cloud of glass particles 1.5 mm dia., and occupying 65% volume of a 2 cm thick bed is considered using the drag law of Crowe et al.[16] The same shock tube geometry[31] is used with no-flux boundary conditions along the side walls, and supersonic outflow in the far extreme of the low pressure region. As before, the initialization is based on a high pressure region to generate the shock wave. The shock tube is 6 m long, with a cross-section of 13 cm x 13 cm, and this is simulated using a 600x13x13 grid. The upstream and downstream pressure traces are presented in Fig. 4, and the simulation results are in good agreement.

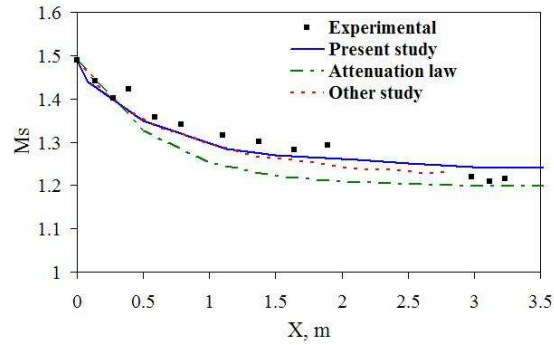

Figure 3. Planar shock wave attenuation in dust-gas suspension.

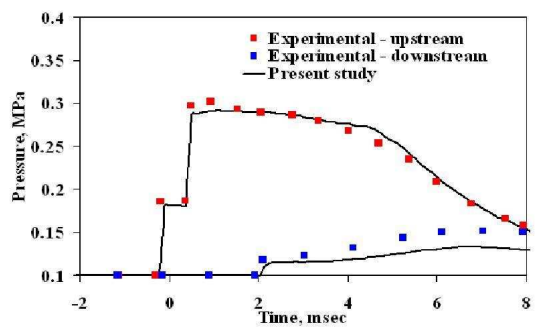

Figure 4. Pressure traces upstream and downstream of a dense particle bed subjected to a shock wave.

IV.D. Detonation without particles

Finally, the detonation of nitromethane from a homogeneous spherical charge is considered. Zhang et al.[3] carried out experiments on detonation of nitromethane from a 11.8 cm dia. glass charge, and measured the blast wave trajectory and the shock front overpressure. Numerical simulations of the same test case are carried out with a sector grid, employing the JWL equation of state for the detonation products. The sector grid is a 20° spherical sector with a domain of 2.4 m in the radial direction, and 2° resolution in the azimuth and zenith directions. A 1000x10x10 grid is employed for the result described below. Earlier studies using different grid resolution and sector dimension showed that in order to get a baseline near-1D solution (as relevant for this baseline comparison) the above noted domain and grid are sufficient.

For the initialization, the gaseous products of nitromethane detonation (CO, H_2O, H_2, N_2) are considered inside the spherical charge. The initial conditions are based on the 1D profiles obtained from the GISPA method[17] described earlier, and these profiles will be shown in the next sub-section along with the profiles for the heterogeneous explosive charge. Fig. 5 shows the primary blast wave trajectory and front overpressure, and the results are in good agreement. As the detonation wave reaches the charge surface, a spherical blast wave is propagated outwards, and an expansion wave inwards. The spherical blast wave attenuates as it propagates. The inward moving expansion wave over-expands the flow, giving rise to a secondary shock. This secondary shock initially moves outwards, comes to a rest, subsequently implodes into the origin, after which, propagates outwards again, trailing behind the primary blast wave. Detailed explanation of these features have been reported elsewhere,[32] and the present results are in good agreement with past observations.

IV.E. Detonation with particles

Detonation modeling is carried out and compared to the experimental data of Zhang et al.[3] An initial heterogeneous charge of 11.8 cm dia., containing nitromethane and steel particles is considered. The steel particles of 463 μm dia., occupy about 63% of the total charge volume and are randomly distributed. The initial explosive conditions are again obtained from the DNS studies and the initial pressure and velocity

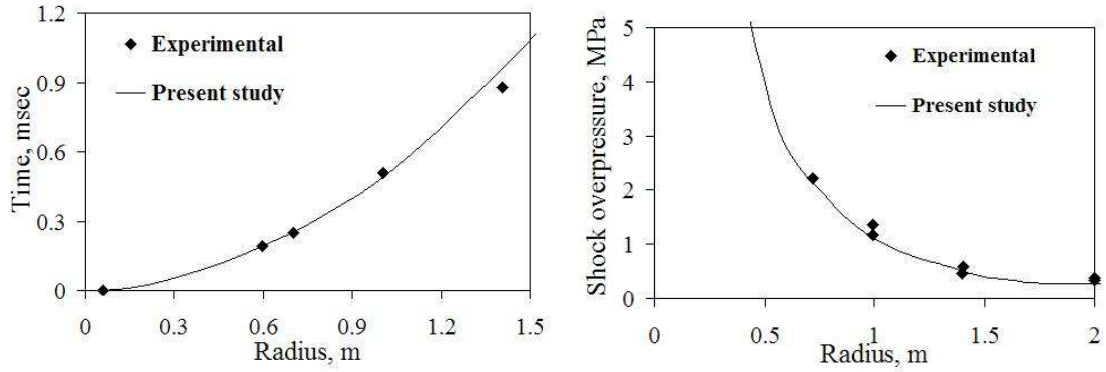

(a) (b)

Figure 5. Nitromethane detonation from a spherical charge (a) blast wave trajectory and (b) front overpressure.

profiles are shown in Fig. 6. Also shown are the profiles for the homogeneous NM charge used for the previous study for comparison.

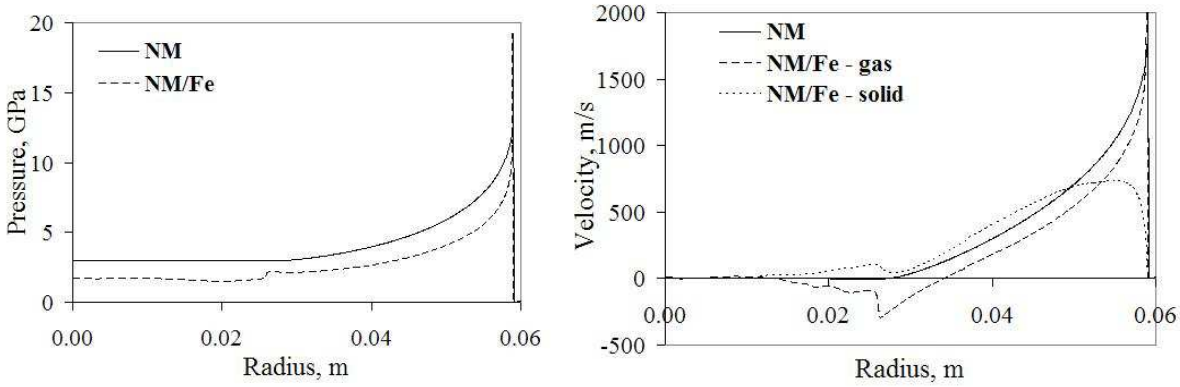

(a) (b)

Figure 6. Initialization for the detonation simulations involving (a) homogeneous and (b) heterogeneous explosive charges.

The same sector domain and grid as employed for the detonation without particles is employed for this study. Fig. 7 shows the sector grid and a close up of the initialization pressure contour, and the initially randomly distributed particle locations. The DEM and the collision model are turned off once the solid particles have dispersed and the flow-field reaches a dilute limit, assumed to be 1% solid volume fraction in this study. This assumed value is based on a comparison of the collision force and the drag force, with the former being at least two orders of magnitude smaller than the latter at such low volume fractions. The drag law and Nusselt number correlations of Akhatov & Vainshtein[33] are used for this study, and the Snider's model[13,14] coefficient, P_s is chosen as 500 MPa, based on an order of magnitude analysis comparing collision and drag forces on a particle. The parameter β is chosen as 3[14] and α_{cs} as 0.9 for the collision model. The blast wave, the particle front trajectories, and the shock overpressure are shown in Fig. 8, and the results are in good agreement with experimental data.

When the detonation wave reaches the charge surface, a blast wave propagates outwards and an expansion wave inwards. The outward moving blast wave decelerates and attenuates as it expands radially outwards. The inward moving expansion accelerates the flow outwards. This process is accompanied by inter-phase drag effects, resulting in acceleration of the particle cloud outwards. During this process, the dense nature

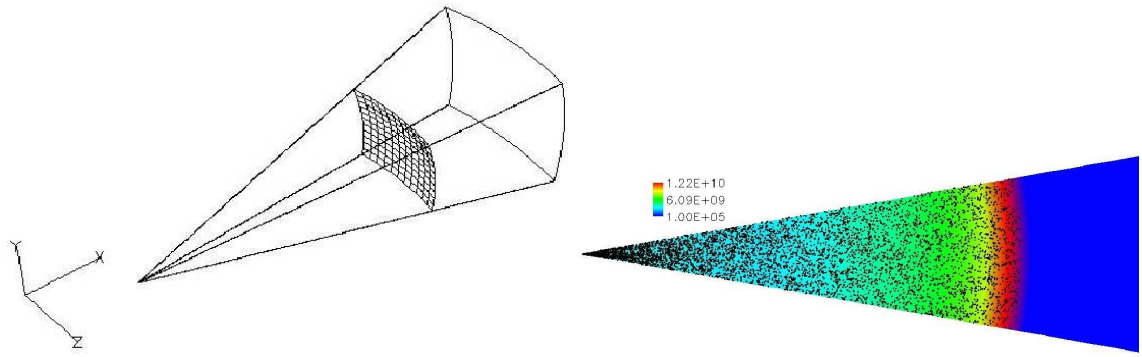

(a) (b)

Figure 7. Initialization for the simulations (a) sector grid and (b) initial pressure contour and particle locations.

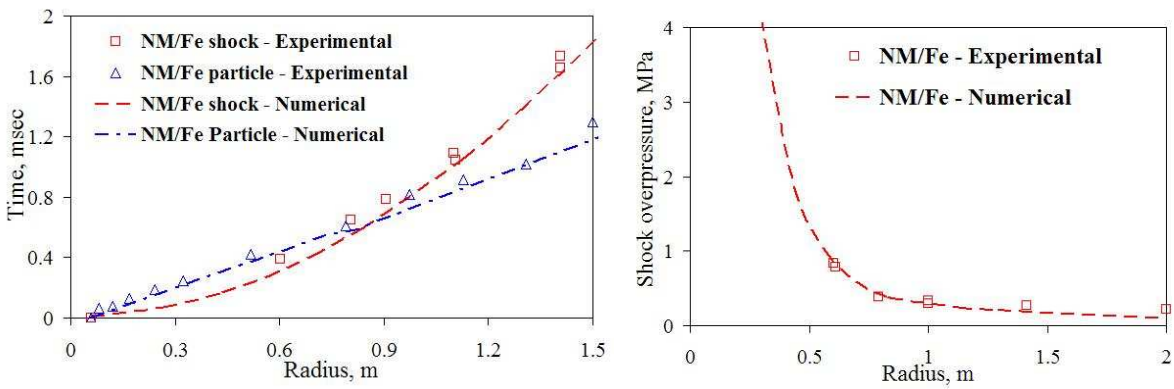

(a) (b)

Figure 8. Nitromethane detonation with steel particles (a) trajectory and (b) shock overpressure.

of the solid particle cloud creates inter-particle collisions/contact, resulting in further outward acceleration of the particles. This is due to the nature of the inter-particle forces trying to lower the dense nature of the explosive charge, which is accomplished only by an outward acceleration of the solid particles.

Analysis of the results show that the inter-particle interaction is dominant over the drag force at early times, and later in time only drag force dominates. This is consistent with results reported in literature[3] (from an order of magnitude analysis, we estimate the net acceleration/deceleration due to collision and drag at early times is on the order of $10^7 m/s^2$). Similar to the homogeneous charge, the inward moving expansion wave over-expands the flow, creating a secondary shock. This secondary shock is initially weak, and is pushed outwards. During this first outward passage, the strength of the secondary shock is augmented as it enters a region of higher pressure, following which, it implodes into the core, due to the low pressure region created by the expansion wave. Subsequently, the secondary shock reflects from the origin and propagates outwards, trailing the primary blast wave. It is observed that the particles at the leading edge of the cloud attain a terminal velocity of around 1300 m/s in about 0.1 msec. This terminal velocity of the solid particles remains nearly constant due to their inertia. At around 0.9 m, the particle cloud front is observed to overtake the shock wave, following which, aerodynamic drag slows down the leading particles. To quantify these observations, the particle velocity histograms are shown at times 0.2, 1.3 and 2 msec in Fig. 9, with bins representing 100 m/s velocity difference. As observed, more particles which are faster than 1000 m/s at 0.2 msec are re-distributed to lower particle velocity bins with time. For the three times considered, more

particle velocity peaks around 500 m/s. We believe that these characteristics will depend on the particle size, nature of the high explosive and the shape and size of the charge used. In the future, we hope to study the problem of interest by varying the suite of identified parameters.

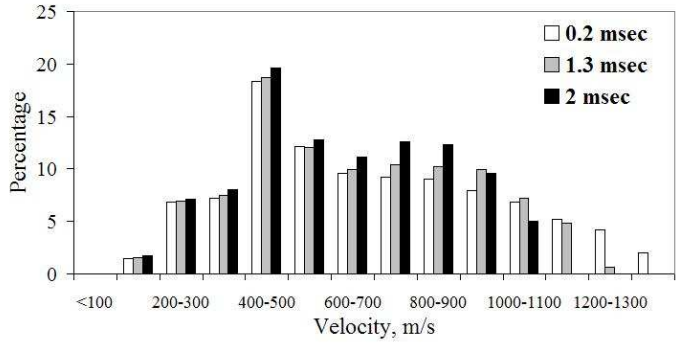

Figure 9. Particle velocity histogram at 0.2, 1.36 and 2 msec.

IV.F. Impulsive loading

The effect of adding solid particles to an explosive as in the heterogeneous NM/Fe charge is compared to a homogeneous NM charge containing the same amount of high explosive. Although both charges contain the same amount of the high explosive, the momentum and heat transfer to the solid particles results in impulse augmentation for the NM/Fe charge, as has been shown by Frost et al.[5] To demonstrate this phenomenon, the pressure and the momentum flux profiles are compared for the two explosive charges at the 0.9 m location in Fig. 10.

As evident from the figure, the pressure is lower for the NM/Fe charge as compared to NM. With the addition of solid particles, momentum and heat transfer from the detonation products to the solid particles results in a slower blast wave for the NM/Fe charge, and a corresponding lower pressure trace. The same argument holds for gas momentum flux profiles. It is observed that the solid momentum flux has a slightly lower peak than the gas momentum flux. Furthermore, the solid momentum flux lasts for a longer time duration than the gas, due to its inertia. These trends have also been reported by Frost et al.[5] Due to the Lagrangian tracking employed for the solid particles, the absence of continuum for the solid phase results in the solid momentum flux profile to be "noisy." Other investigators[5] assumed the solid particles to be in continuum, thereby obtained a smooth profile for the solid momentum flux. However, we will show that the total impulse estimates with the non-continuum assumption (Eulerian-Lagrangian) results in similar trends as with the continuum assumption (Eulerian-Eulerian[5]).

In order to better understand the transfer of momentum from the gas to the particles, four different groups of particles are considered. 100 particles initially occupying radial locations between (0.058 ± 0.001) m are randomly chosen, and this group is named C58. Similar groups of 100 particles each are considered, initially occupying radial locations between (0.048 ± 0.001) m, (0.038 ± 0.001) m and (0.028 ± 0.001) m and named C48, C38 and C28, respectively. The average velocity of all the 100 solid particles belonging to each group, and the average local gas velocity as seen by each group are plotted in Fig. 11. As evident from the figure, the order of terminal velocities is C58 > C48 > C38 > C28, with the differences narrowing down between adjacent groups at smaller initial radial locations. This is due to an outer group being more free to move outwards than an inner one, which is constrained by the dense cloud of particles. Another observation is that the terminal velocity is reached within about 0.1 msec for all the groups, indicating the preponderance of the inter-particle interaction force, which is dominant at early times. Another reason for the rapid attainment of the terminal velocity is the drag coefficient (and drag force) on the particles, which is higher in a dense cloud than in the dilute limit. The symbols in the figures indicate the times at which half the number of particles belonging to the corresponding group have penetrated the shock front. As evident from the figure, the average particle velocity of C58 and C48 starts to decrease after penetrating the shock front. Furthermore, it is also evident that C58 slows down more than C48 upon penetration. This is due to the fact that C58, after penetration, enters ambient atmosphere, and is subjected to high aerodynamic drag. However, when C48 penetrates the shock front, it encounters lesser aerodynamic drag, as the particles ahead of it have imparted a certain amount of flow to the ambient air. C38 and C28 are not observed to penetrate

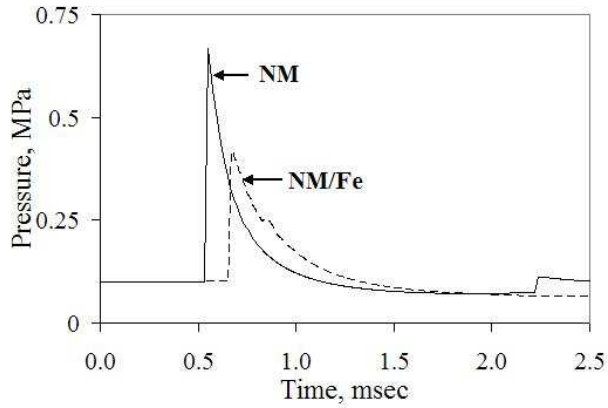

(a)

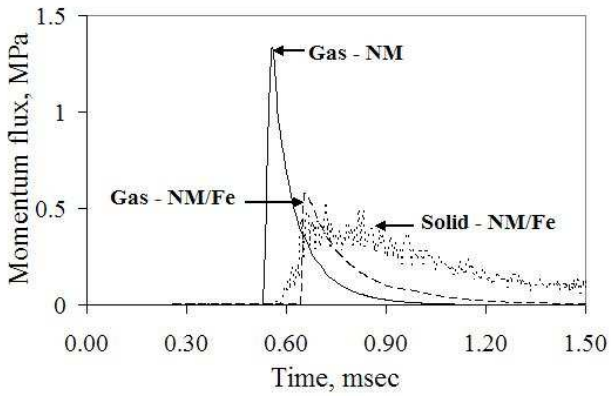

(b)

Figure 10. (a) pressure and (b) momentum flux profiles for NM and NM/Fe charges at 0.9 m.

the shock front in the time duration of study. From the average local gas velocity as seen by each group, it is evident that each group initially encounters different average local gas velocities, in the order C58 > C48 > C38 > C28. Particles closer to the outer surface of the charge encounter higher local gas velocities due to the rapidly expanding gas, caused by the inward moving rarefaction wave. After an initial plateau, it is observed that the local gas velocities fall off, earlier ($\approx$ 0.25 msec) for C58, but slightly later for the other groups, due to the faster travelling C58. For C48, C38 and C28, a second plateau is observed in the local average gas velocity, as they approach the blast wave. Furthermore, the particles ahead of these groups start to decelerate, thereby transfering momentum back to the gas phase, and can also contribute to the flat second plateau observed for C48, C38 and C28. The second plateau lasts for a longer time for C38 and C28, as compared with C48, as the former two groups take a longer time to catch up with the primary blast wave due to their slower motion. Whether C38 and C28 eventually catch up with the primary blast wave could not be ascertained, as the primary blast wave is observed to reach the end of the simulation domain before these inner groups.

The total deliverable impulse from a heterogeneous (or a homogeneous) charge can be estimated from the simulation data and typically, will be due to three components, i.e., pressure, gas and particle momentum fluxes. These quantities can be integrated in time to obtain the total deliverable impulse. Some investigators[34,35] have considered the impulse due to excess gas pressure and particle momentum only, while others have considered the bending of a cantilever rod to quantify impulse.[5] In this paper, our interest is on the impulse deliverable to a "virtual wall" since the physical wall is not included in the current simulation. We

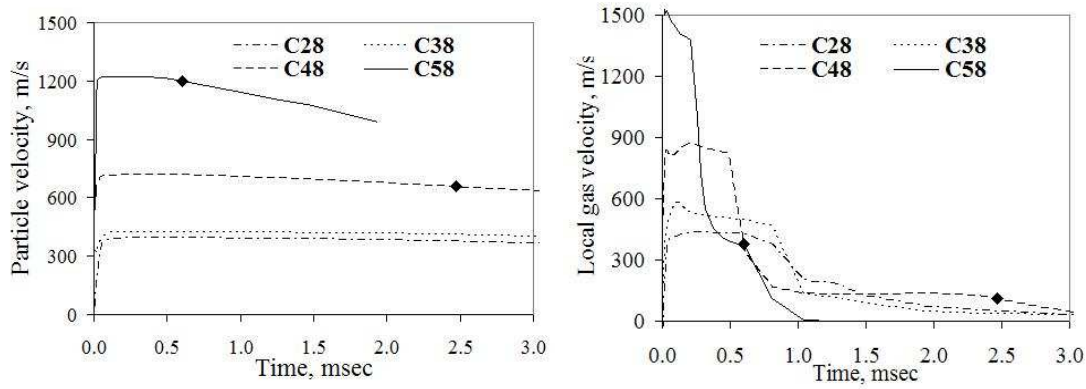

(a) (b)

Figure 11. (a) average particle velocity and (b) average local gas velocity for different groups of particles.

define the total impulse (I) as:

$$I = \int_0^\infty (p_g - p_o)_{p_g > p_o} dt + \int_0^\infty \frac{1}{2}\rho_g \alpha_g {u_g}^2 dt + \rho_p \int_0^\infty \frac{1}{2}\alpha_p {u_p}^2 dt, \tag{13}$$

where p_0 denotes the ambient pressure. The impulse due to pressure, gas and particle momentum flux are denoted as I_p, I_{gm} and I_{pm}, respectively. I_{pm} is computed as a summation over all the particles present in a small control volume around the radial distance of interest. The total impulse and its three components are shown in Fig. 12 (a). Also shown is the ratio, I_{pm}/I_{gm}. The expansion of the gas and particle phases with radius causes the total impulse to decrease. I_{pm} is larger than I_{gm} at all radius, by a factor of about 3-4. Similar trends have been reported by other investigators.[5] In Fig. 12 (b), the impulse between the NM and NM/Fe charges containing the same amount of the high explosive are compared at different radial locations. As evident from the figure, impulse augmentation for the NM/Fe charge over the NM charge decreases from a factor of 2.5 in the near-field (4 charge dia.) to about 1.2 in the far-field (20 charge dia.). Thus, the advantage of adding solid particles to an explosive charge is more pronounced in the near-field, and asymptotes towards unity in the far-field. At farther distances from the charges, the significant slowing down of the solid particles negates any impulse augmentations, thereby tending the behavior of a heterogeneous charge to that of a point source homogeneous charge. We believe that these characteristics will depend on many variables, such as the charge shape, the particle size, loading and material properties, and the choice of the high explosive. However, the simulation model developed here can be used for systematic evaluation of these properties and their impact on the observed features. Such a study is currently underway and will be reported in the near future.

The impulsive loading predictions for the NM and NM/Fe charges containing the same amount of the high explosive can be used for damage assessment, albeit in a crude sense. Our impulse predictions does not consider physical phenomena such as blast wave reflection and diffraction, and particle collision with a structure. However, impulse values reported in literature for the destructibility of a 0.23 m thick brick wall, aircraft wing and aircraft skin[36–38] fall within the same range as in the current estimation. Thus, simulations such as these can be used as a first approximation for damage assessment.

IV.G. Sensitivity to collision model coefficient

For the heterogeneous blast wave simulations performed hitherto, the collision model coefficient, P_s was chosen as 500 MPa, based on an order of magnitude analysis of the drag and collision forces on a particle. In order to better elucidate the sensitivity of the results on the collision model coefficient, another simulation was carried out with the collision model coefficient turned off, i.e. $P_s = 0$. It was observed that the primary and secondary blast wave trajectories and overpressure are unaffected by the choice of the collision model coefficient. The particle front trajectory was observed to be slightly faster for the higher collision model coefficient, albeit to a very small extent. However, considering the slight scatter in the available experimental

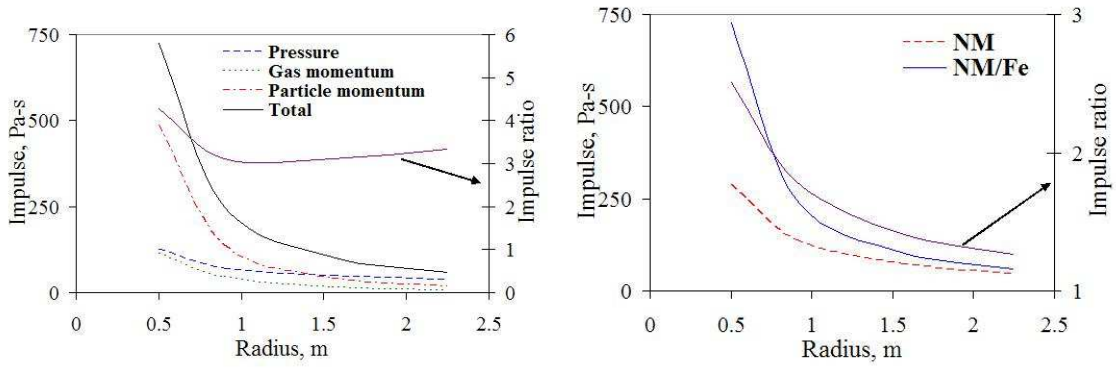

(a) (b)

Figure 12. (a) Total impulse and its components and (b) comparison between NM and NM/Fe charges.

data,[3] the particle front for both cases are within this scatter. The pressure and gas momentum fluxes were observed to be only slightly affected for both choices of P_s. For the sake of brevity, these observations are not presented here. A slightly more pronounced difference was observed in the solid momentum flux, and is shown in Fig. 13 at the 0.9 radial location. Although for both cases the solid momentum flux begins to rise around 0.6 msec at the 0.9 m location, the peak is observed to be higher with the collision/contact model turned on. With the model turned on, a few more particles are concentrated towards the leading edge of the cloud, due to the collision force at earlier times, resulting in the observed higher peak. Between 1 and 1.6 msec, the trends for the two cases are observed to be similar. At around 1.8 msec, a small second peak is observed with the collision model turned on. Although this second peak has not been reported by other investigators,[5] we believe that this second peak is owing to the slight "kink" observed in the heterogeneous initial detonation profile (Fig. 6) for the gas and solid particles. This kink affects the particle concentration, which in turn causes collisions that can redistribute the particles locally. This local redistribution is obviously not observed with the collision model turned off. Beyond 2.3 msec, both profiles seem to again follow the same trends. In spite of these differences, the total impulse was observed to be only about 10% higher with the collision model turned on.

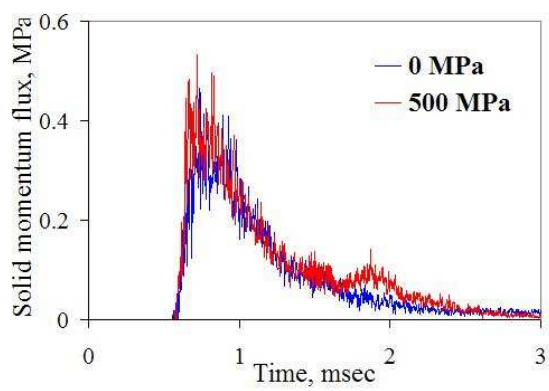

Figure 13. Solid momentum flux for P_s = 0 and 500 MPa.

V. Conclusions

Simulation of flow and particle motion associated with the interaction of a detonation wave with dense heavy inert particles has been investigated. This is achieved with the use of a new Eulerian-Lagrangian two-

phase model capable of capturing the initial dense phase clustering effects and the interactions of particles with shock and the gas phase. Several validation studies have been carried out to establish the accuracy of the hydrocode. The pressure, velocity and momentum flux distributions are used to estimate the total impulse at different radial locations. The heterogeneous charge is found to deliver an impulse of about 2.5 times a homogeneous charge containing the same amount of the high explosive in the near-field but only slightly more in the far-field. The current study has demonstrated a robust simulation model that can be used for studies of detonations including dense inert particles. Extension to handle reacting particles is not difficult since the solver already has reacting flow capability. Future studies will focus on more detailed evaluation of the sensitivity of the post detonation structure on the explosive initial charge configuration, including the properties of the particles.

Acknowledgments

This research is supported by the Office of Naval Research (Dr. Cliff Bedford, Dr. Judah Goldwasser) and the Eglin Air Force Base (Dr. Doug Nance). Simulations were performed at the Naval Oceanographic Major Shared Resource Center. The first author also acknowledges the private discussions with Dr. Richard Saurel of Polytech Marseille, France, on the development of the DEM.

References

[1]Lanovets, V. S., Levich, V. A., Rogov, N. K., Tunik, Y. V., and Shamshev, K. N., "Dispersion of the Detonation Products of a Condensed Explosive with Solid Inclusions," *Combustion, Explosion and Shock Waves*, Vol. 29, No. 5, 1993, pp. 638–641.

[2]Milne, A. M., "Detonation in Heterogeneous Mixtures of Liquids and Particles," *Shock Waves*, Vol. 10, 2000, pp. 351–362.

[3]Zhang, F., Frost, F. D., Thibault, P. A., and Murray, S. B., "Explosive Dispersal of Solid Particles," *Shock Waves*, Vol. 10, 2001, pp. 431–443.

[4]Zhang, F., Thibault, P. A., and Link, R., "Shock Interaction with Solid Particles in Condensed Matter and Related Momentum Transfer," *Proceedings: Mathematical, Physical and Engineering Sciences*, Vol. 459, No. 2031, 2003, pp. 705–726.

[5]Frost, D. L., Ornthanalai, C., Zarei, Z., Tanguay, V., and Zhang, F., "Particle Momentum Effects from the Detonation of Heterogeneous Explosives," *Journal of Applied Physics*, Vol. 101, No. 113529, 2007.

[6]Massoni, J., Saurel, R., Lefrancois, A., and Baudin, G., "Modeling Spherical Explosions with Aluminized Energetic Materials," *Shock Waves*, Vol. 16, 2006, pp. 75–92.

[7]Abgrall, R. and Saurel, R., "Discrete Equations for Physical and Numerical Compressible Multiphase Mixtures," *Journal of Computational Physics*, Vol. 186, 2003, pp. 361–396.

[8]Chinnayya, A., Daniel, E., and Saurel, R., "Modelling Detonation Waves in Heterogeneous Energetic Materials," *Journal of Computational Physics*, Vol. 196, 2004, pp. 490–538.

[9]Le Metayer, O., Massoni, J., and Saurel, R., "Modelling Evaporation Fronts with Reactive Riemann Solvers," *Journal of Computational Physics*, Vol. 205, 2005, pp. 567–610.

[10]Cowperthwaite, M., "Significance of Some Equations of State Obtained From Shock-Wave Data," *American Journal of Physics*, Vol. 34, n. 11, 1966, pp. 1025–1030.

[11]Zukas, J. A and Walters, W. P., *Explosive Effects and Applications,* Springer, 1998.

[12]Toro, E. F., *Riemann Solvers and Numerical Methods for Fluid Dynamics*, Springer, 1999.

[13]Snider, D. M., "An Incompressible Three-Dimensional Multiphase Particle-in-Cell Model for Dense Particle Flows," *Journal of Computational Physics*, Vol. 170, 2001, pp. 523–549.

[14]Patankar, N. A. and Joseph, D. D., "Modeling and Numerical Simulation of Particulate Flows by the Eulerian-Lagrangian Approach," *International Journal of Multiphase Flow*, Vol. 27, 2001, pp. 1659–1684.

[15]Gonthier, K. A. and Powers, J. M, "A High-Resolution Numerical Method for a Two-Phase Model of Deflagration-to-Detonation Transition," *Journal of Computational Physics*, Vol. 163, 2000, pp. 376–433.

[16]Crowe, C., Sommerfeld, M., and Tsuji, Y., *Multiphase Flows with Droplets and Particles*, CRC Press, 1998.

[17]Nance, D. V., *Private Communication*, 2007.

[18]Xu, S., Aslam, T. and Stewart, D. S., "High Resolution Numerical Simulation of Ideal and Non-ideal Compressible Reacting Flows with Embedded Internal Boundaries," *Combustion Theory and Modeling*, Vol. 1, 1997, pp. 113–142.

[19]Xu, S. and Stewart, D. S., "Deflagration-to-detonation Transition in Porous Energetic Materials: a Comparative Model Study," *Journal of Engineering Mathematics*, Vol. 31, 1997, pp. 143–172.

[20]Wescott, B. L., Stewart, D. S. and Davis, W. C., "Equation of State and Reaction Rate for Condensed Phase Explosives," *Journal of Applied Physics*, Vol. 98, 2005, 053514.

[21]Hayes, D. B., "A P^nt Detonation Criterion from Thermal Explosion Theory," *Sixth Intrenational Symposium on Detonation, Pasadena, CA*, 1976.

[22]Glaister, P., "An Approximate Linearized Riemann Solver for the Euler Equations for Real Gases," *Journal of Computational Physics*, Vol. 74, 1998, pp. 382–408.

[23]Bdzil, J. B., Stewart, D. S. and Jackson, T. L., "Program Burn Algorithms Based on Detonation Shock Dynamics: Discrete Approximations of Detonation Flows With Discontinuous Front Models," *Journal of Computational Physics*, Vol. 174, 2001, pp. 870–902.

[24]Menon, S. and Patel, N., "Subgrid Modeling for Simulation of Spray Combustion in Large-Scale Combustors," *AIAA Journal*, Vol. 44, No. 5, 2006, pp. 709–723.

[25]Devals, C., Jourdan, G., Estivalezes, J. L., Meshkov, E. E., and Houas, L., "Shock Tube Spherical Particle Accelerating Study for Drag Coefficient Determination," *Shock Waves*, Vol. 12, 2003, pp. 325–331.

[26]Igra, O. and Takayama, K., "Shock Tube Study of the Drag Coefficient of a Sphere in a Non-stationary Flow," *Proc. Royal Society of London A*, Vol. 442, 1993, pp. 231–247.

[27]Clift, R., Grace, J. R., and Weber, M. E., *Bubbles, Drops and Particles*, Academic, New York, 1978.

[28]Sommerfeld, M., "The Unsteadiness of Shock Waves Propagating Through Gas-Particle Mixtures," *Experiments in Fluids*, Vol. 3, 1985, pp. 197–206.

[29]Aizik, F., Ben-Dor, G., Elperin, T., Igra, O., Mond, M., and Gronig, H., "Attenuation Law of Planar Shock Waves Propagating Through Dust-Gas Suspensions," *AIAA Journal*, Vol. 33, No. 5, 1995, pp. 953–955.

[30]Chang, E. J. and Kailasanath, K., "Shock Wave Interactions with Particles and Liquid Fuel Droplets," *Shock Waves*, Vol. 12, 2003, pp. 333–341.

[31]Rogue, X., Rodriguez, G., Haas, J. F., and Saurel, R., "Experimental and Numerical Investigation of the Shock-induced Fluidization of a Particles Bed," *Shock Waves*, Vol. 8, 1998, pp. 29–45.

[32]Brode, H. L., "Blast Wave From a Spherical Charge," *The Physics of Fluids*, Vol. 2, 1959, pp. 217–229.

[33]Akhatov, I. Sh. and Vainshtein, P. B., "Transition of Porous Explosive Combustion Into Detonation," *Combustion, Explosion and Shock Waves*, Vol. 20, No. 1, 1984, pp. 63–69.

[34]Ivandaev, A. I. and Kutushev, A. G., "Influence of Screening Gas-suspension Layers on Shock Wave Reflection," *Journal of Applied Mechanics and Technical Physics*, Vol. 26, 1985, pp. 103–109.

[35]Kruglikov, B. S. and Kutushev, A. G., "Attenuation of Air Shock Waves by Layers of Dusty Gas and Lattices," *Journal of Applied Mechanics and Technical Physics*, Vol. 29, 1988, pp. 48–53.

[36]Bulson, P. S., *Explosive Loading of Engineering Structures*, E & FN Spon, 1978.

[37]Zalosh, R. G., *Industrial Fire Protection Engineering*, pp. 34, Wiley, 2003.

[38]Kinney, G. F. and Graham, K. J., *Explosive Shocks in Air*, Springer-Verlag, 1985.

[39]Kuhl, A. L., "Mixing in Explosions," *Russian Academy of Sciences technical meeting, Moscow, Russia*, 1993.

[40]Frost, D. L., Zarei, Z. and Zhang, F., "Instability of Combustion Products Interface from Detonation of Heterogeneous Explosives," *Proceedings of 20th International Colloquium on the Dynamics of Explosions and Reactive Systems, Montreal, Canada*, 2005.

[41]Turns, S. R., *An Introduction to Combustion,* McGraw-Hill Publishing Co, 2000.

[42]Fickett, W. and Davis, W. C., *Detonation Theory and Experiment,* Dover Publications, 2000.